Microviscometry reveals reduced blood viscosity and altered shear rate and shear stress profiles in microvessels after hemodilution

David S. Long[†], Michael L. Smith[‡], Axel R. Pries[§], Klaus Ley[‡¶], and Edward R. Damiano[†‖]

[†]Department of Mechanical and Industrial Engineering, University of Illinois at Urbana–Champaign, Urbana, IL 61801; [‡]Department of Biomedical Engineering and [¶]Cardiovascular Research Center, University of Virginia Health Science Center, Charlottesville, VA 22908; and [§]Department of Physiology, Charité Universitätsmedizin, 14195 Berlin, Germany

Communicated by William R. Schowalter, Princeton University, Princeton, NJ, April 27, 2004 (received for review July 20, 2003)

We show that many salient hemodynamic flow properties, which have been difficult or impossible to assess in microvessels *in vivo*, can be estimated by using microviscometry and fluorescent microparticle image velocimetry in microvessels >20 μm in diameter. Radial distributions in blood viscosity, shear stress, and shear rate are obtained and used to predict axial pressure gradient, apparent viscosity, and endothelial-cell surface-layer thickness *in vivo*. Based solely on microparticle image velocimetry data, which are readily obtainable during the course of most intravital microscopy protocols from systemically injected particle tracers, we show that the microviscometric method consistently predicted a reduction in local and apparent blood viscosity after isovolemic hemodilution. Among its clinical applications, hemodilution is a procedure that is used to treat various pathologies that require reduction in peripheral vascular-flow resistance. Our results are directly relevant in this context because they suggest that the fractional decrease in systemic hematocrit is ≈25–35% greater than the accompanying fractional decrease in microvascular-flow resistance *in vivo*. In terms of its fundamental usefulness, the microviscometric method provides a comprehensive quantitative analysis of microvascular hemodynamics that has applications in broad areas of medicine and physiology and is particularly relevant to quantitative studies of angiogenesis, tumor growth, leukocyte adhesion, vascular-flow resistance, tissue perfusion, and endothelial-cell mechanotransduction.

Dating back to the work of Fåhræus over 70 years ago, studies related to blood flow in the microcirculation (1–4) have been featured prominently in scientific investigations across various fields, including endothelial-cell mechanotransduction, inflammation, vascular permeability, angiogenesis, and tissue engineering. Nevertheless, no method has been developed for either quantitatively predicting or measuring the salient dynamic, kinematic, and rheological properties of microvascular blood flow *in vivo* other than in the single-file flow regime within capillaries of 5–8 μm in diameter (4–7). All attempts at analyzing microvascular blood-flow properties in microvessels above the capillary range have depended on knowledge of quantities, such as the axial pressure gradient within the vessel and the red-cell concentration of blood discharged by the vessel, which are essentially unknown in these vessels (2, 3, 8, 9). In the absence of any satisfactory way of estimating these hemodynamic quantities, researchers have had to resort to indirect methods, which often contain errors of nearly an order of magnitude.

In 1830, the physiologist J. L. M. Poiseuille arrived at his celebrated law relating the volumetric flow rate of a Newtonian fluid in a cylindrical tube to the difference in pressure acting across the length of the tube (10). A century later, Fåhræus and Lindqvist showed that, because of the phase separation between red cells and plasma that occurs in microvessels and glass capillary tubes (11), an increasing departure from Poiseuille's law is observed with decreasing diameter (12). However, although they were able to establish this fact, which has come to be known as the Fåhræus–Lindqvist effect, the means for predicting blood-flow parameters on theoretical grounds in either glass capillary tubes or microvessels beyond the single-file flow regime eluded scientists working in this area for the remainder of the century.

Because red blood cells are less concentrated near the wall than near the center of microvessels, mean red-cell velocity exceeds mean plasma velocity. This disparity in mean velocities gives rise to the so-called Fåhræus effect, which is associated with a decrease in the instantaneous volume fraction of red cells in the vessel or tube hematocrit, H_T, relative to the red-cell concentration discharged from the vessel, or discharge hematocrit, H_D. In general, neither H_T nor H_D are equal to the systemic hematocrit, H_{sys}, which is obtained from a large artery or vein, because red cells and plasma distribute unevenly at microvascular bifurcations (13). Measurements of H_T in microvessels *in vivo* have been attempted either by using microphotometric methods (8, 14) or by counting labeled red cells (15), neither of which are reliable in microvessels more than ≈20 μm in diameter. Measurements of H_D have been attempted in microvessels *in vivo* either by micropipette aspiration and centrifugation (16), which is extremely cumbersome and feasible only in some tissues, or by a microphotometric method (13), which assumes the same Fåhræus effect in glass tubes and microvessels of the same size. The accuracy of this assumption, however, is dubious in light of recent evidence of the influence of the endothelial surface layer (ESL) on plasma flow near the wall of microvessels *in vivo* (17, 18). In addition to the difficulties associated with determining H_T and H_D *in vivo*, attempts (8, 19) at measuring or estimating either axial pressure gradient or flow resistance accurately in microvessels have been unsuccessful *in vivo*.

The central tenet of our approach (20), which we hereafter shall refer to as the microviscometric method, is that distributions in the local viscosity, $\mu(r)$, as a function of the radial position, r, over the cross section of glass capillary tubes and microvessels, can be determined analytically from the cross-sectional axial velocity distribution, $v_z(r)$, where $v_z(r)$ can be extracted from particle tracers in the flow by using intravital fluorescent microparticle image velocimetry (μ-PIV) (17, 21, 22). In addition to the viscosity distribution, $\mu(r)$, we can use the microviscometric method to predict quantitatively various flow parameters in microvessels *in vivo*, including axial pressure gradient, dp/dz; volume flow rate, Q; and the relative apparent blood viscosity, η_{rel}, defined as the ratio of steady volume–flow rates per unit pressure drop of blood plasma relative to whole blood. The velocity distribution, $v_z(r)$, is related kinematically to the shear rate distribution, $\dot{\gamma}(r) = dv_z/dr$, where $\dot{\gamma}(r)$ is assumed

Abbreviations: μ-PIV, microparticle image velocimetry; ESL, endothelial surface layer.

‖To whom correspondence should be addressed. E-mail: damiano@uiuc.edu.

www.pnas.org/cgi/doi/10.1073/pnas.0402937101

to be related constitutively to the shear stress distribution, $\tau(r) = \mu(r)\ \dot{\gamma}(r)$, for a linearly viscous fluid. By means of rigorous analysis of glass-tube experiments *in vitro*, where pressure gradient and feed hematocrit can be measured directly, and isovolemic hemodilution experiments *in vivo*, where the change in systemic hematocrit is known, we provide quantitative validation of the microviscometric method and show a decrease in local and apparent blood viscosity in individual microvessels as a direct result of reducing systemic hematocrit.

Materials and Methods

Analytical Methods. The analysis (20) on which the microviscometric method is based invokes the continuum approximation and regards the heterogeneous red-cell suspension as a homogeneous, continuously varying, and linearly viscous incompressible fluid that has a spatially nonuniform viscosity distribution (23) over the vessel cross section. Cokelet (2) found support for the continuum approximation in his studies by using physiological concentrations of red blood cells suspended in plasma flowing at physiological shear rates in glass tubes as small as 20 μm in diameter. As for our constitutive assumption, our results are consistent with the linearly viscous approximation because, as we will show, over most of the tube or vessel cross section, shear rates are more than $\approx 50\ s^{-1}$ under physiologically typical flow rates. Blood viscosity at a given hematocrit is nearly constant at such shear rates (24). Thus, we assume that at shear rates of more than $\approx 50\ s^{-1}$, blood is Newtonian in the sense that local viscosity depends only on local thermodynamic state and local hematocrit and is independent of shear rate.

It is further assumed that, in postcapillary venules, the flow is steady and the velocity profile is axisymmetric and fully developed. A brief summary of the analysis of an axisymmetric, fully developed, and steady incompressible flow of a linearly viscous fluid having a spatially varying viscosity distribution over the cross section of both cylindrical glass tubes and ESL-lined microvessels is provided in *Supporting Text*, which is published as supporting information on the PNAS web site. Full details are given in ref. 20.

Glass-Tube Experiments. Fluorescent μ-PIV (21, 22) was performed by using a method described in ref. 17. Fluoresbrite yellow–green microspheres (0.47 ± 0.01 μm, 1.05 g/cm^3; Polysciences) were visualized by using stroboscopic double-flash (5- to 16.67-ms apart; Strobex 11360, Chadwick–Helmuth, El Monte, CA) epi-illumination, and recordings were made by using a VE-1000CD charge-coupled device camera (Dage–MTI, Michigan City, IN) on an S-VHS recorder (Panasonic, Secaucus, NJ).

The *in vitro* perfusion system consisted of a 3-ml feed reservoir and a horizontally mounted glass capillary tube (length, 27.5, 26.2, and 20 mm; i.d., 54.2, 50.7, and 81.0 μm, respectively), which were connected by a microhematocrit tube (i.d., 1.2 mm) and silastic tubing (Dow-Corning), to a 10-ml downstream reservoir that could be manipulated vertically with a Vernier caliper (Nolan Supply, Syracuse, NY) (17, 25). To account for the unavoidable mismatch of refractive indices between the perfusate and the inner tube wall, the radial position of every microsphere was corrected by using Snell's law (17). Human blood samples were obtained from healthy volunteers by means of venipuncture, anticoagulated with heparin (final concentration, 10 units/ml), and used within 2–4 h after withdrawal. The buffy coat was discarded after centrifugation, and erythrocytes were resuspended in plasma. The hematocrit of each sample, which was adjusted to one of five nominal values between 0% and 60%, was determined by using a Hemavet 850 cell counter (CDC Technologies, Oxford, CT).

Intravital Experiments. Male mice (C57BL/6) obtained from The Jackson Laboratory were prepared for intravital microscopy by following the methods described in ref. 17. All animal experiments were conducted under a protocol approved by the University of Virginia Institutional Animal Care and Use Committee (protocol no. 2474). All mice appeared to be healthy and were 8–14 weeks of age. Microscopic observations of microspheres *in vivo* were made in venules of the exteriorized cremaster muscle and followed the *in vitro* protocols described above and in *Supporting Text*. No optical correction of the radial positions of microspheres measured *in vivo* was necessary because the difference in the refractive indices of blood plasma and the surrounding tissue is negligibly small (17).

Hemodilution. Mice were given a 1.0-ml i.p. injection of physiological saline to help prevent fluid imbalance before cremaster exteriorization. During hemodilution, the carotid artery cannula was allowed to bleed into an inverted syringe tube for accurate volume measurements. Saline was infused through the jugular vein cannula at a volume flow rate matched to the carotid bleed rate until 0.75 ml was exchanged. Blood samples (30 μl) were drawn from the carotid artery at least 25 min before and after hemodilution for systemic hematocrit measurements. Up to two vessels per animal were recorded before and after hemodilution and analyzed offline by using the microviscometric method, as described above and in *Supporting Text*. Exact vessel locations were noted by using muscle striations as markers.

Data Analysis. Video recordings were digitized with PREMIERE software (Adobe Systems, Mountain View, CA; final resolution 5.43 pixels per μm) and then analyzed with the public domain National Institutes of Health IMAGE program (available at http://rsb.info.nih.gov/nih-image), as described in refs. 17 and 26. The flash-time interval for μ-PIV recordings was chosen such that the two images for a given microsphere were 3- to 30-μm apart. The center-to-center distance between these two images and the shortest distance between the microsphere center and the vessel or tube wall were measured for $\approx$75 microspheres in each glass capillary tube and $\approx$50 microspheres in each microvessel. Measurements were restricted to a section of capillary tube or microvessel <180 μm or 15 μm in axial length, respectively. Each μ-PIV data set was used to extract an axisymmetric velocity profile, $v_z(r)$, by following the methods described in *Supporting Text*.

Results

To test the validity of the microviscometric method in a model system, we obtained fluorescent μ-PIV data over the cross section of glass capillary tubes (i.d., $\approx$50–80 μm) that were perfused steadily with saline, plasma, and red-cell suspensions in plasma, as described above. Distributions predicted in glass capillary tubes by using the microviscometric method were qualitatively similar to those shown in Fig. 1 (see Figs. 5–14, which are published as supporting information on the PNAS web site). For red-cell suspensions, results consistently revealed a concentrated red-cell core and a cell-poor region near the vessel wall (see Figs. 5–12). Furthermore, the shear-rate distributions consistently showed a nearly linear variation over $\approx$50–70% of the tube cross section around the center of the tube and a highly nonlinear variation near the tube wall (see Figs. 1 and 5–12). The nearly parabolic velocity distributions and linear shear rate distributions predicted in saline-perfused glass tubes (see Figs. 1 *A* and *C*, 13, and 14) after optically correcting the measured radial position of each microsphere provide confidence in the optical correction procedure that we used for all of our glass-tube μ-PIV data. Further validation is provided in ref. 17.

Evidence to support the validity of the microviscometric method *in vitro* is shown in Fig. 2, in which directly measured

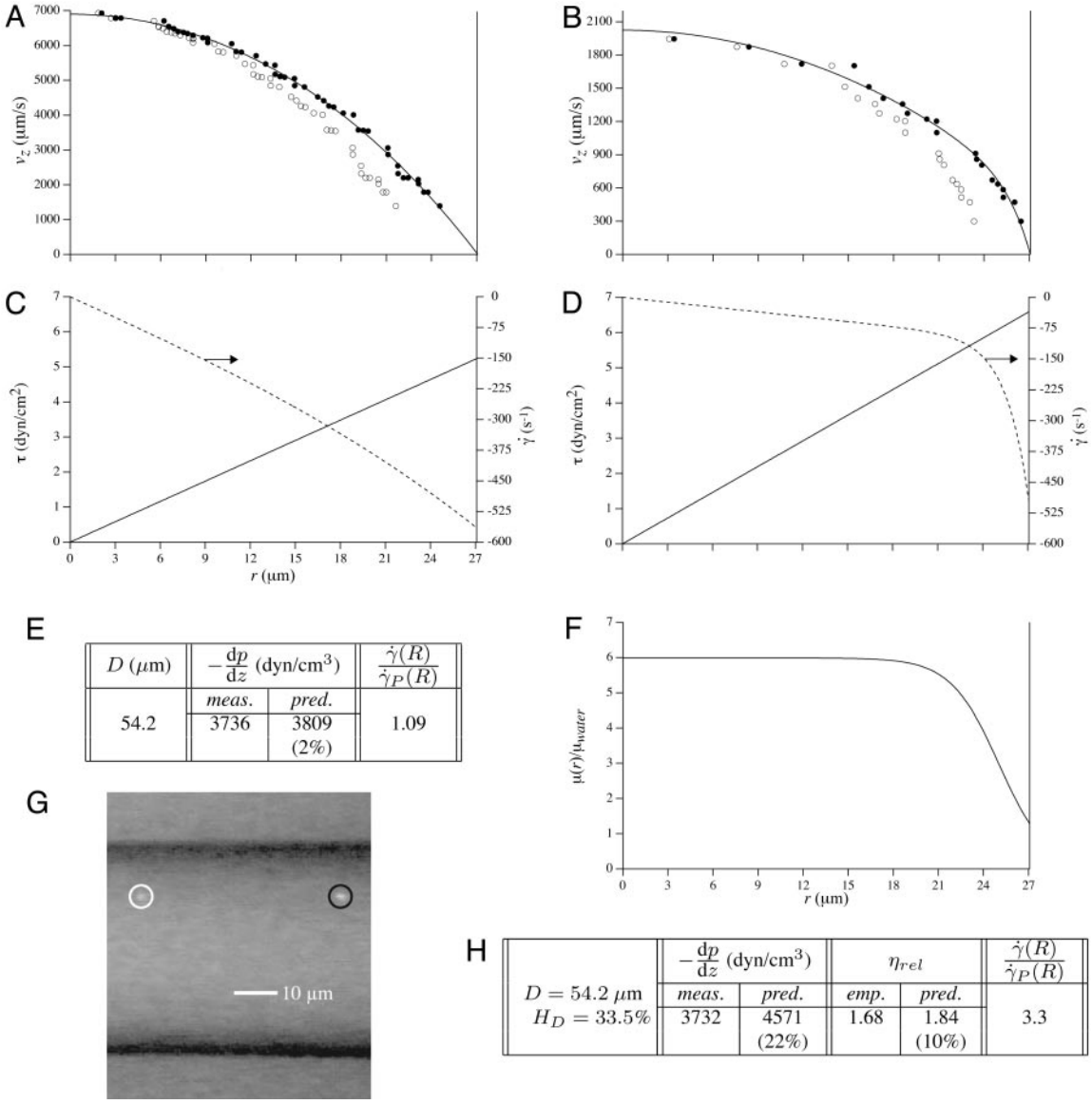

D (μm)	$-\frac{dp}{dz}$ (dyn/cm^3)		$\frac{\dot{\gamma}(R)}{\dot{\gamma}_P(R)}$
	meas.	*pred.*	
54.2	3736	3809 (2%)	1.09

	$-\frac{dp}{dz}$ (dyn/cm^3)		η_{rel}		$\frac{\dot{\gamma}(R)}{\dot{\gamma}_P(R)}$
	meas.	*pred.*	*emp.*	*pred.*	
$D = 54.2$ μm, $H_D = 33.5\%$	3732	4571 (22%)	1.68	1.84 (10%)	3.3

Fig. 1. Optically corrected fluorescent (●) and raw (○) μ-PIV data obtained from a 54.2-μm-diameter glass tube steadily perfused with saline (*A*) and washed red cells suspended in plasma (*B*) (human blood, $H_D = 33.5\%$). Superimposed on the μ-PIV data in *A* and *B* are axisymmetric velocity distributions, $v_z(r)$, extracted from the data by following the methods described in ref. 20. (*C* and *D*) Distributions in shear rate (dashed curves, right axes) and shear stress (solid curves, left axes) over the tube cross section, corresponding to the velocity distributions shown in *A* and *B*. (*F*) Predicted distribution in the normalized viscosity, $\mu(r)/\mu_{water}$, derived by using the analytical expression for $\mu(r)$ (see *Supporting Text*). (*E* and *H*) Geometric and rheological quantities associated with *A* and *B*, respectively, including the measured tube diameter, D, and discharge hematocrit, H_D; the measured and predicted values of the axial pressure gradient, dp/dz; and the ratio of the predicted wall shear rate, $\dot{\gamma}(R)$, to the wall shear rate, $\dot{\gamma}_P(R)$, of a Poiseuille flow, having the centerline velocities shown in *A* and *B*. Also tabulated in *H* are the empirically estimated (3) and predicted values of the relative apparent viscosity, η_{rel}. Percentages given in parentheses under each of the predicted values listed in the tables correspond to the percentage of difference between measured (or empirically estimated) and predicted values. (*G*) Bright-field image of the saline-perfused glass tube referenced in *A* showing dual images of one microsphere (upstream, white circle; downstream, black circle) separated in time by the double-flash interval.

values of dp/dz and empirically estimated (3) values of η_{rel} agree closely with their corresponding values predicted by using the microviscometric method for each μ-PIV data set. Furthermore, these results provide support for the validity of using the continuum approximation of blood to obtain estimates of dp/dz and η_{rel} in glass capillary tubes $\approx$50 μm in diameter.

To apply the microviscometric method to blood flow in microvessels *in vivo*, a generalization is introduced (20) to account for the hemodynamic influence of the ESL (17, 18, 27, 28). Expressions for $\mu(r)$ and dp/dz apply in microvessels (see *Supporting Text*) if the tube radius, R, is replaced by a, where a is the radial location of the effective hydrodynamic interface between the blood in the lumen and the ESL (17, 20). It is assumed that red cells and particle tracers do not invade the ESL (7, 17, 28–30) and that plasma flow through the ESL can be well approximated with the Brinkman equation (17, 20, 29, 31, 32), where the hydraulic resistivity, K, of the ESL is taken to be more than $\approx 10^9$ dyn·s/cm^4 (1 dyn = 10 μN) (7, 17, 29, 30). The thickness, $R - a$, of the ESL is estimated by following the methods described in ref. 20, in which the value of a is determined by minimizing the least-squares error in the fit to the μ-PIV data. The minimum least-squares error for the 12 microvessels that we analyzed (i.d., 34.2 $\pm$ 1.7 μm) occurred over ESL thicknesses ranging 0.29–0.71 μm, with an average thick-

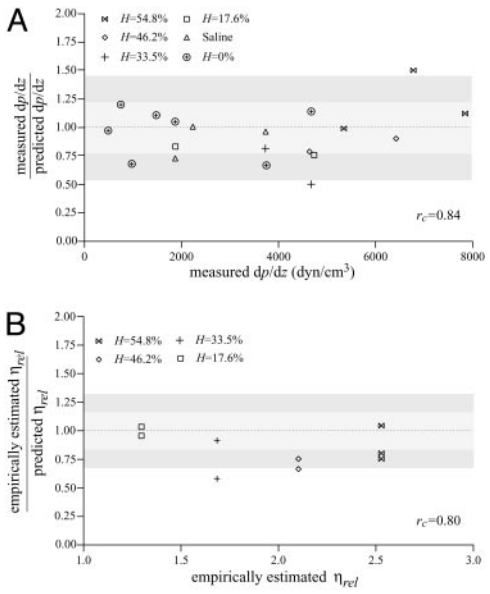

Fig. 2. Predictability of dp/dz and η_{rel} by using microviscometric analysis of μ-PIV data obtained from glass capillary tubes *in vitro*. Ratio of the measured to predicted value of dp/dz versus the corresponding measured value (*A*) and ratio of the empirically estimated (3) to predicted value of η_{rel} versus the corresponding empirically estimated value (*B*). Predicted values were determined by applying the microviscometric method to the μ-PIV data obtained from the glass-tube experiments. The light and dark shaded regions span, respectively, one and two standard deviations in the distributions around unity. The standard deviation corresponds to 23% for dp/dz and 16% for η_{rel}. The correlation coefficient, r_c, is shown for its corresponding predicted quantity.

ness of $\approx 0.51 \pm 0.04$ μm for $K = 10^9$ dyn·s/cm^4 (see Table 1 and Figs. 15–26, which are published as supporting information on the PNAS web site). By contrast, the least-squares error associated with *in vitro* μ-PIV data increased monotonically with increasing $R - a > 0$ (see Figs. 5–12), which is consistent with the fact that no ESL is present in glass tubes. In each of the microvessels that we analyzed, ESL thickness estimates showed little sensitivity to values of $K > 10^9$ dyn·s/cm^4 (see *D* in Figs. 15–26).

As an example, Fig. 3 shows the results of one *in vivo* hemodilution experiment in a mouse cremaster-muscle venule (diameter, ≈ 40 μm). Results for other hemodilution experiments are shown in Figs. 27–31 and Table 2, which are published as supporting information on the PNAS web site. To facilitate a quantitative comparison between the results of our hemodilution experiments and quantities that can be predicted by the microviscometric method, we define μ_T^*, which is analogous to tube hematocrit, H_T, and μ_D^*, which is analogous to discharge hematocrit, H_D, where

$$\mu_T^* := \frac{1}{A}\int\int_A \frac{\mu(r)}{\mu_a}\,dA, \qquad \mu_D^* := \frac{1}{Q}\int\int_A \frac{\mu(r)}{\mu_a}\,v_z(r)dA, \qquad [1]$$

A is the cross-sectional area of the vessel lumen, Q is the volume flow rate in the vessel, and $\mu_a = \mu(a)$. The analogous quantities, H_T and H_D, correspond to the mean instantaneous red-cell concentration in the vessel and the mean red-cell flux fraction through the vessel, respectively (see *Supporting Text*). It is evident from Eq. **1** that μ_T^* corresponds to the mean instantaneous normalized viscosity over the vessel cross section, whereas for a unit volume flow rate, μ_D^* is simply the product of the local viscosity (which depends on the local red-cell concentration) and the local volume flow rate integrated over the vessel cross section. If both $v_z(r)$ and $\mu(r)$ are positive functions over the vessel cross section and decrease monotonically with increasing radial position, it will always be the case that $\mu_T^*/\mu_D^* < 1$, just as the Fåhræus effect implies that $H_T/H_D < 1$. The relative apparent viscosity, η_{rel}, however, is a measure of flow resistance of whole blood relative to blood plasma.

If the species-specific transport relationship, $H(\mu)$, were available for mouse blood, the distribution $\mu(r)/\mu_a$ could be replaced by $H[\mu(r)]$ in Eq. **1** to provide expressions for H_T and H_D (see *Supporting Text*). In the absence of such data, we cannot estimate H_T or H_D directly; however, we can nevertheless use Eq. **1** to quantitatively evaluate the accuracy of the microviscometric method *in vivo* by noting that the percentage of decrease in μ_D^* would likely be very similar to the percentage of decrease in its counterpart, H_D (and likewise for μ_T^* and its counterpart, H_T), because the transport relationship enters into the integrand of each term in the numerator of the percentage of decrease in H_D in the same way as it does in the denominator. That is, we assume that $[(\mu_D^*)_i - (\mu_D^*)_f]/(\mu_D^*)_i \approx [(H_D)_i - (H_D)_f]/(H_D)_i$, where *i* and *f* refer a particular quantity to its value in the same vessel before and after systemic hemodilution, respectively.

To test the validity of this assumption quantitatively, we again turn to the results of our glass-tube experiments in which H_D is known. We can regard any pair of glass-tube experiments having different measured values of H_D as an "*in vitro* hemodilution experiment," in which the higher and lower values of H_D in the pair can be thought of as corresponding to before and after hemodilution, respectively. Substituting the distribution $\mu(r)$ predicted from the microviscometric method into Eq. **1**, we have determined μ_T^* and μ_D^* for each of our glass-tube experiments involving red-cell suspensions in plasma. For any two glass-tube experiments having different measured values of H_D, the accuracy with which we can predict the percentage of difference in the directly measured values of H_D from the percentage of difference in our predicted values of μ_D^* is shown in Fig. 4. It is evident from these results that, even without knowledge of the specific transport relationship, $H(\mu)$, we can indirectly infer the percentage of difference in H_D from our predictions of the percentage of difference in μ_D^* with an accuracy that is similar to that which was achieved in our direct predictions of the rheological quantities shown in Fig. 2.

Having established, in glass tubes, the accuracy with which the percentage of change in μ_D^* can be used to infer the percentage of change in H_D, provides some measure of confidence for using this metric *in vivo*. Further support, however, can be found directly from our *in vivo* hemodilution experiments (see Figs. 3 and 27–31) by comparing the average percentage of decrease in μ_D^* with the average percentage of decrease in H_{sys} after isovolemic hemodilution (see Table 2). In all five vessels analyzed *in vivo*, μ_T^* and μ_D^* decreased after systemic hemodilution. For an average decrease in H_{sys} of $33.5 \pm 1.0\%$, the average percentage of decrease in μ_T^* and μ_D^* (and, by inference, H_T and H_D) across all five vessels was predicted to be 33.5 ± 5.2 and $36.3 \pm 4.8\%$, respectively. Because red-cell screening and plasma skimming at vessel branch points gives rise to network heterogeneity in the discharge hematocrits of individual microvessels, the percentage of decrease in H_D for any individual microvessel is not, in general, equal to the percentage of decrease in the systemic hematocrit of the animal. Although it was impractical to measure the percentage of decrease in H_D directly after hemodilution in each of the vessels that we analyzed, there is evidence that in microvessels more than ≈ 20 μm in diameter, the average discharge hematocrit across N microvessels in a network does indeed approach the systemic hematocrit with increasing N (13). Hence, the mean fractional decrease in μ_D^* should approach the mean fractional decrease in H_{sys} as the number of analyzed

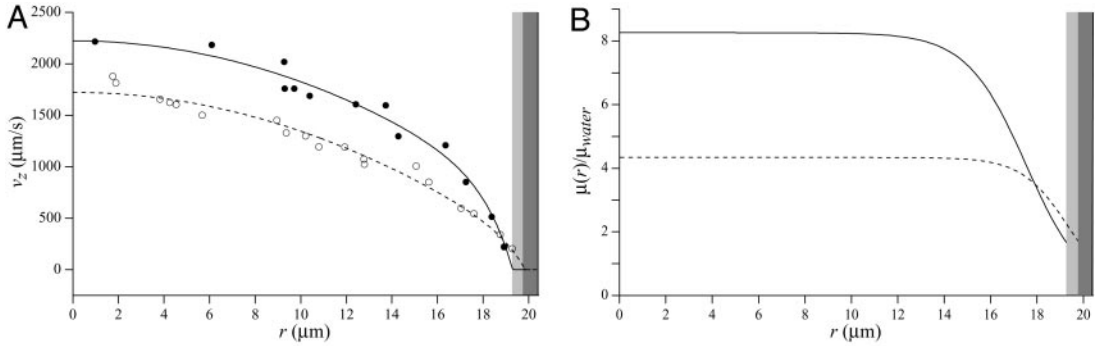

C

% decrease in μ_T^* $\left(\frac{1}{A}\iint_A \frac{\mu(r)}{\mu_a}\,dA\right)$	% decrease in μ_D^* $\left(\frac{1}{Q}\iint_A \frac{\mu(r)}{\mu_a}\,v_z(r)\,dA\right)$	% decrease in η_{rel}	% decrease in H_{sys}
39.4	43.5	26.0	34.6

D

D (μm)	$R-a$ (μm)	$-\frac{dp}{dz}$ (dyn/cm^3)	η_{rel}	$\frac{\dot\gamma(a)}{\dot\gamma_P(R)}$
40.2	0.82	8,724	3.08	3.4

E

D (μm)	$R-a$ (μm)	$-\frac{dp}{dz}$ (dyn/cm^3)	η_{rel}	$\frac{\dot\gamma(a)}{\dot\gamma_P(R)}$
40.9	0.64	4,386	2.28	2.3

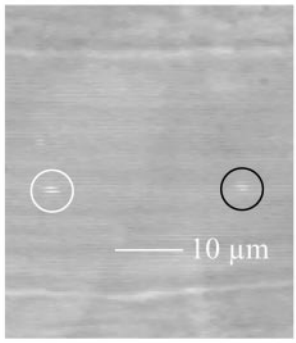

Fig. 3. Results of a microviscometric analysis of μ-PIV data obtained from a mouse cremaster venule during one hemodilution experiment. Intravital fluorescent μ-PIV data with predicted velocity profiles (*A*) and normalized viscosity profiles (*B*) in a venule (diameter, ≈40 μm) of the mouse cremaster muscle before (●, solid curves) and after (○, dotted curves) systemic hemodilution. Curves shown have the same interpretation as those shown in Fig. 1. The shaded regions near the vessel wall represent the ESL before (light gray) and after (dark gray) systemic hemodilution, where the ESL is modeled as a Brinkman medium (20, 31, 32) having a hydraulic resistivity, $K = 10^9$ dyn·s/cm^4. The thickness of the ESL is estimated by minimizing the normalized least-squares error associated with the fit to the μ-PIV data (see Figs. 5–12), as described in ref. 20. Tabulated in *C* for this vessel is the percentage of decrease after systemic hemodilution in μ_T^*, μ_D^*, η_{rel}, and the systemic hematocrit, H_{sys}. Parameters tabulated for before (*D*) and after (*E*) hemodilution include the measured vessel diameter, *D*; the estimated ESL thickness, $R-a$, corresponding to $K = 10^9$ dyn·s/cm^4; the predicted axial pressure gradient, dp/dz; the predicted relative apparent viscosity, η_{rel}; and the ratio of the predicted interfacial shear rate, $\dot\gamma(a)$, to the wall shear rate, $\dot\gamma_P(R)$, of a Poiseuille flow having the centerline velocity associated with the profiles shown in *A*. (*F*) Bright-field image of a venule showing dual images of one microsphere (upstream, white circle; downstream, black circle) separated in time by the double-flash interval.

vessels increases. This trend is observed in the *in vivo* results presented here.

As with μ_T^* and μ_D^*, our microviscometric analysis predicted that in every vessel that we analyzed, flow resistance, as measured by the relative apparent viscosity, η_{rel}, was also seen to decrease (25.1 ± 6.1%, on average) after systemic hemodilution.

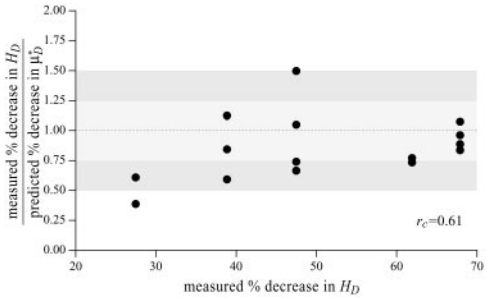

Fig. 4. Ratio of the measured percentage of decrease in H_D to the predicted percentage of decrease in μ_D^* versus the corresponding measured percentage of decrease in H_D. Predicted values were determined by applying Eq. **1** and the microviscometric method to the μ-PIV data obtained from the glass-tube experiments. The light and dark shaded regions span, respectively, one and two standard deviations in the distributions around unity, where the standard deviation corresponds to 25%. The correlation coefficient, r_c, is 0.61.

Collectively, these results provide the first direct and quantitative estimate of the accompanying fractional decrease in local and apparent blood viscosity in individual microvessels that is associated with the clinically relevant procedure of isovolemic hemodilution.

A noteworthy trend observed in these results is that the average percentage of decrease in measured H_{sys} and predicted μ_D^* were, respectively, 33% and 45% greater than the average percentage of decrease in predicted η_{rel} *in vivo*. This trend was observed also in our glass-tube studies, in which the average percentage of decrease in measured H_D and predicted μ_D^* were, respectively, 26% and 48% greater than the average percentage of decrease in predicted η_{rel}. This trend has potentially important clinical implications in the context of hemodilution procedures because it is the decrease in η_{rel}, and not the decrease in H_D or H_{sys}, that quantitatively determines the decrease in microvascular-flow resistance. Thus, these results suggest that the fractional decrease in systemic hematocrit is ≈25–35% greater than the accompanying fractional decrease in microvascular-flow resistance.

Discussion

By using fluorescently labeled platelets as endogenous particle tracers, previous work has revealed blunted velocity profiles in microvessels *in vivo* and showed that the Poiseuille flow approximation underestimates wall shear rate in these microvessels (21,

23). However, those results were not analyzed rigorously to yield all of the distributions and rheological parameters estimated here, nor could they have been, because the particle tracers that were used were too large to provide the necessary spatial resolution. Furthermore, these earlier studies did not account for the ESL, which was not well documented at the time. In fact, the near complete retardation of plasma by the ESL adjacent to the vessel wall causes fluid shear stress and fluid shear rate at the luminal endothelial-cell surface [i.e., wall shear rate, $\dot{\gamma}(R)$, and wall shear stress, $\tau(R)$] to be very nearly zero for values of hydraulic resistivity more than $\approx 10^9$ dyn·s/cm^4 (17). Consequently, these results show that the appropriate quantitative metrics characterizing near-wall microfluidics in microvessels are the interfacial shear rate, $\dot{\gamma}(a)$, and interfacial shear stress, $\tau(a) = \mu_a \dot{\gamma}(a)$, which can now be predicted by using the microviscometric method.

The most popular and widespread method for estimating microvascular blood-flow parameters *in vivo* is the dual-slit technique, which uses mean blood-flow velocity, derived from centerline velocity measured by cross correlation (8, 33), to estimate wall shear rate. Most studies make this estimate by assuming a Poiseuille flow in the microvessel and imposing the no-slip condition at the vessel wall. However, as these results show, under physiologically typical discharge hematocrits and flow rates, the interfacial shear rate, $\dot{\gamma}(a)$, corresponding to the shear rate at the effective interface between the ESL and the free lumen, is, on average, about five times greater than estimates of wall shear rate based on the dual-slit technique assuming Poiseuille flow (see Table 1).

Microrheological phenomena in terminal vascular beds impact broad areas of medicine and physiology. We have demonstrated that the microviscometric method allows estimation of the axial pressure gradient and relative apparent viscosity of steady flows in microvessels 20–50 μm in diameter, without the need to impale these vessels with micropipettes and without any prior assumptions about the Fåhræus or Fåhræus–Lindqvist effects *in vivo*. Because the experimental methods used to obtain μ-PIV data are compatible with most intravital microscopy protocols, the microviscometric method can provide a systematic, standardized approach by which microvascular-flow parameters can be estimated *in vivo*. The radial distributions in viscosity, shear stress, and shear rate predicted here, as well as the means for determining them, will allow detailed quantitative modeling of the hemodynamics of microvascular networks *in vivo*. Furthermore, the ability of the microviscometric method to detect the presence of the ESL and estimate its hydrodynamically relevant thickness in microvessels >20 μm in diameter is essential to the quantitative aspects of a broad range of fields in microvascular physiology. In particular, by using the microviscometric method before and after various treatments to degrade the ESL (17, 18, 20, 28, 34), we are now poised to gain insight into the role of the ESL in inflammation, endothelial-cell mechanotransduction, microvascular hemodynamics, and flow-mediated mechanisms in angiogenesis (27). Finally, by using the microviscometric method before and after isovolemic hemodilution, we have directly demonstrated the impact of this procedure on hemodynamics in individual microvessels. These results have direct clinical relevance because systemic hemodilution has been used to save blood during surgery and to reduce peripheral resistance, and it is sometimes used in the treatments of Ménières disease, polycythemia vera, sickle-cell anemia, and newborns with a systemic hematocrit in excess of $\approx$70%. Because data similar to the data underlying the present analysis can be obtained in many organs and tissues, including those that are not transparent and require fluorescent epi-illumination, it is likely that data sets with broad applicability to physiology and pathophysiology will now become available.

We thank A. L. Butterworth for assistance in data acquisition from video tape. This work was supported by Whitaker Foundation Grant TF-02-0024, National Science Foundation Grant BES-0093985 (to E.R.D.), and National Institutes of Health Grants HL64381 and T32GM 08715-01A1 (to K.L.).

1. Goldsmith, H. L. (1986) *Microvasc. Res.* **31,** 121–142.
2. Cokelet, G. R. (1999) *Biorheology* **36,** 343–358.
3. Pries, A. R., Neuhaus, D. & Gaehtgens, P. (1992) *Am. J. Physiol.* **263,** H1770–H1778.
4. Secomb, T. W., Skalak, R., Özkaya, N. & Gross, J. F. (1986) *J. Fluid. Mech.* **163,** 405–423.
5. Damiano, E. R. (1998) *Microvasc. Res.* **55,** 77–91.
6. Secomb, T. W., Hsu, R. & Pries, A. R. (1998) *Am. J. Physiol.* **274,** H1016–H1022.
7. Secomb, T. W., Hsu, R. & Pries, A. R. (2001) *Am. J. Physiol.* **281,** H629–H636.
8. Lipowsky, H. H., Kovalcheck, S., Zweifach, B. W. (1978) *Circ. Res.* **43,** 738–749.
9. Sharan, M., Popel, A. S. (2001) *Biorheology* **38,** 415–428.
10. Poiseuille, J. L. M. (1830) *J. Physiol. Exp. Pathol.* **10,** 277–295.
11. Fåhræus, R. (1928) *Klin. Wochenschr.* **7,** 100–106.
12. Fåhræus, R. & Lindqvist, T. (1931) *Am. J. Physiol.* **96,** 562–568.
13. Pries, A. R., Ley, K. & Gaehtgens, P. (1986) *Am. J. Physiol.* **251,** H1324–H1332.
14. Jendrucko, R. J. & Lee, J. S. (1973) *Microvasc. Res.* **6,** 316–331.
15. Sarelius, I. H. & Duling, B. R. (1982) *Am. J. Physiol.* **243,** H1018–H1026.
16. Desjardins, C. & Duling, B. R. (1987) *Am. J. Physiol.* **252,** H494–H503.
17. Smith, M. L., Long, D. S., Damiano, E. R. & Ley, K. (2003) *Biophys. J.* **85,** 637–645.
18. Pries, A. R., Secomb, T. W., Jacobs, H., Sperandio, M. B., Osterloh, K. & Gaehtgens, P. (1997) *Am. J. Physiol.* **273,** H2272–H2279.
19. Pries, A. R., Secomb, T. W., Gessner, T., Sperandio, M. B., Gross, J. F. & Gaehtgens, P. (1994) *Circ. Res.* **75,** 904–915.
20. Damiano, E. R., Long, D. S. & Smith, M. L. (2004) *J. Fluid Mech.* **512,** 1–19.
21. Tangelder, G. J., Slaaf, D. W., Muijtjens, A. M., Arts, T., oude Egbrink, M. G. & Reneman, R. S. (1986) *Circ. Res.* **59,** 505–514.
22. Santiago, J. G., Wereley, S. T., Meinhart, C. D., Beebe, D. J. & Adrian, R. J. (1998) *Exp. Fluids* **25,** 316–319.
23. Bugliarello, G. & Hayden, J. W. (1963) *Trans. Soc. Rheol.* **7,** 209–230.
24. Chien, S., Usami, S., Taylor, H. M., Lundberg, J. L. & Gregersen, M. I. (1966) *J. Appl. Physiol.* **21**, 81–87.
25. Alonso, C., Pries, A. R., Kiesslich, O., Lerche, D. & Gaehtgens, P. (1995) *Am. J. Physiol.* **268,** H25–H32.
26. Norman, K. E. (2001) *Microcirculation* **8,** 243–249.
27. Pries, A. R., Secomb, T. W., Gaehtgens, P. (2000) *Pflügers Arch.* **440,** 653–666.
28. Vink, H. & Duling, B. R. (1996) *Circ. Res.* **79,** 581–589.
29. Feng, J. & Weinbaum, S. (2000) *J. Fluid Mech.* **422,** 281–317.
30. Damiano, E. R. & Stace, T. M. (2002) *Biophys. J.* **82,** 1153–1175.
31. Damiano, E. R., Duling, B. R., Ley, K. & Skalak, T. C. (1996) *J. Fluid Mech.* **314,** 163–189.
32. Damiano, E. R., Long, D. S., El-Khatib, F. H. & Stace, T. M. (2004) *J. Fluid Mech.* **500,** 75–101.
33. Baker, M. & Wayland, H. (1974) *Microvasc. Res.* **7,** 131–143.
34. Desjardins, C. & Duling, B. R. (1990) *Am. J. Physiol.* **258,** H647–H654.

Corrections and Retraction

CORRECTIONS

BIOPHYSICS. For the article "Microviscometry reveals reduced blood viscosity and altered shear rate and shear stress profiles in microvessels after hemodilution," by David S. Long, Michael L. Smith, Axel R. Pries, Klaus Ley, and Edward R. Damiano, which appeared in issue 27, July 6, 2004, of *Proc. Natl. Acad. Sci. USA* (**101,** 10060–10065; first published June 25, 2004; 10.1073/pnas.0402937101), the first two authors, David S. Long and Michael L. Smith, contributed equally to this work.

www.pnas.org/cgi/doi/10.1073/pnas.0406339101

INAUGURAL ARTICLE, DEVELOPMENTAL BIOLOGY. For the article "Nuclear cloning of embryonal carcinoma cells," by Robert H. Blelloch, Konrad Hochedlinger, Yasuhiro Yamada, Cameron Brennan, Minjung Kim, Beatrice Mintz, Lynda Chin, and Rudolf Jaenisch, which appeared in issue 39, September 28, 2004, of *Proc. Natl. Acad. Sci. USA* (**101,** 13985–13990; first published August 11, 2004; 10.1073/pnas.0405015101), all authors agree to this correction. The mouse embryonal carcinoma cell line referred to in the publication as METT-1 was in fact a derivative designated METT-1a, and it should have been referred to as such throughout the paper. The METT-1 cell line was isolated from an induced teratocarcinoma and found to be karyotypically normal (29). When injected into blastocysts, the cells contributed to all somatic tissues and to the germ line (25). The cells in the present study were grown from a thawed aliquot of the METT-1 line, previously tested *in vivo* and frozen at culture passage 12 (25). In the experiments we performed, the cells were grown in a medium different from the one to which they had been adapted, and they were passaged repeatedly to obtain the data reported in the present study. Genetic and developmental differences, relative to METT-1, may have arisen during these passages. This correction does not change the conclusions in the present study.

25. Stewart, T. A. & Mintz, B. (1981) *Proc. Natl. Acad. Sci. USA* **78,** 6314–6318.
29. Mintz, B. & Cronmiller, C. (1981) *Somatic Cell Genet.* **7,** 489–505.

www.pnas.org/cgi/doi/10.1073/pnas.0406245101

RETRACTION

BIOCHEMISTRY. For the article "Molecular dissection of the roles of nucleotide binding and hydrolysis in dynein's AAA domains in *Saccharomyces cerevisiae*," by Samara L. Reck-Peterson and Ronald D. Vale, which appeared in issue 6, February 10, 2004, of *Proc. Natl. Acad. Sci. USA* (**101,** 1491–1495; first published January 30, 2004; 10.1073/pnas.2637011100), the undersigned authors wish to note the following: "In conjunction with a follow-up project regarding these mutations, we resequenced several of the mutant yeast strains and found that the genes in two of the eight analyzed mutant strains (the E2488Q mutation in the AAA3 domain and the K2766A mutation in the AAA4 domain) no longer contained the mutation and instead were wild type. The correct K2766A mutation does not have a defect in either nuclear segregation or microtubule dissociation as originally reported; however, there is a modest defect (≈50% decrease) in microtubule binding. More significantly, the true E2488Q mutation demonstrated a severe nuclear segregation phenotype and a defect in the release of dynein from microtubules with ATP, comparable to that reported for the nuclear hydrolysis mutation in AAA1. Thus, our initial conclusion that the AAA site 3 ATP hydrolysis mutation has no phenotype is incorrect. We now know that ATP hydrolysis in both AAA1 and AAA3 is essential for dynein function and that nucleotide binding at AAA2 and AAA4 is necessary for maximal levels of microtubule binding *in vitro*."

Samara L. Reck-Peterson
Ronald D. Vale

www.pnas.org/cgi/doi/10.1073/pnas.0404506101